

## Gold Nanorod Linking to Control Plasmonic Properties in Solution and Polymer Nanocomposites

Robert C. Ferrier, Jr.,<sup>†</sup> Hyun-Su Lee,<sup>‡,§,||</sup> Michael J. A. Hore,<sup>‡</sup> Matthew Caporizzo,<sup>‡</sup> David M. Eckmann,<sup>§,||</sup> and Russell J. Composto\*,<sup>‡</sup>

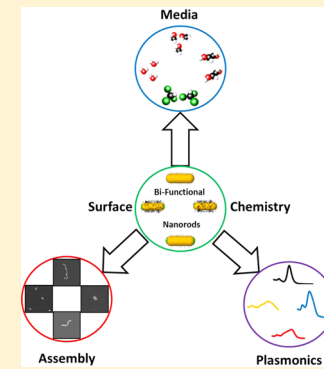
<sup>†</sup>Department of Chemical and Biomolecular Engineering, University of Pennsylvania, 220 South 33rd Street, Philadelphia, Pennsylvania 19104, United States

<sup>‡</sup>Department of Materials Science and Engineering and the Laboratory for Research on the Structure of Matter, University of Pennsylvania, 3231 Walnut Street, Philadelphia, Pennsylvania 19104, United States

<sup>§</sup>Institute of Medicine and Engineering and <sup>||</sup>Department of Anesthesiology and Critical Care, University of Pennsylvania, 3620 Hamilton Walk, Philadelphia, Pennsylvania 19104, United States

### Supporting Information

**ABSTRACT:** A novel, solution-based method is presented to prepare bifunctional gold nanorods (B-NRs), assemble B-NRs end-to-end in various solvents, and disperse linked B-NRs in a polymer matrix. The B-NRs have poly(ethylene glycol) grafted along its long axis and cysteine adsorbed to its ends. By controlling cysteine coverage, bifunctional ligands or polymer can be end-grafted to the AuNRs. Here, two dithiol ligands (C6DT and C9DT) are used to link the B-NRs in organic solvents. With increasing incubation time, the nanorod chain length increases linearly as the longitudinal surface plasmon resonance shifts toward lower adsorption wavelengths (i.e., red shift). Analogous to step-growth polymerization, the polydispersity in chain length also increases. Upon adding poly(ethylene glycol) or poly(methyl methacrylate) to chloroform solution with linked B-NR, the nanorod chains are shown to retain end-to-end linking upon spin-casting into PEO or PMMA films. Using quartz crystal microbalance with dissipation (QCM-D), the mechanism of nanorod linking is investigated on planar gold surfaces. At submonolayer coverage of cysteine, C6DT molecules can insert between cysteines and reach an areal density of 3.4 molecules per nm<sup>2</sup>. To mimic the linking of Au NRs, this planar surface is exposed to cysteine-coated Au nanoparticles, which graft at 7 NPs per μm<sup>2</sup>. This solution-based method to prepare, assemble, and disperse Au nanorods is applicable to other nanorod systems (e.g., CdSe) and presents a new strategy to assemble anisotropic particles in organic solvents and polymer coatings.



### INTRODUCTION

Controllably assembled plasmonic nanoparticles hold promise as the functional components for a tunable sensing platform, such as one based upon surface enhanced Raman spectroscopy (SERS),<sup>1,2</sup> as well as optical polarizers<sup>3,4</sup> and antennae.<sup>5</sup> In addition to their facile synthesis,<sup>6,7</sup> gold nanorods (AuNRs) are particularly attractive for these applications because particle anisotropy as well as AuNR spacing and orientation impart assemblies of AuNRs with unique optical properties.<sup>8</sup> AuNRs have been assembled in both side-by-side and end-to-end alignments by modifying the surface with small linker molecules<sup>9–13</sup> or polymers<sup>14,15</sup> and/or by adjusting solvent conditions.<sup>16</sup> Whereas these approaches achieve some control over spacing, orientation, and, therefore, optical properties of the AuNRs, these strategies are restricted to water or mixed water/organic solvent solutions, thereby limiting possible device fabrication processing. Furthermore, the full potential of assembled AuNRs requires casting them into a processable medium, such as a polymer, that produces well-dispersed AuNRs. Although individual AuNRs have been cast in polymer matrices in random orientations,<sup>17</sup> they have yet to be

assembled as discrete chains and dispersed within a polymer matrix. The aim of this research is to develop a strategy to control the end-to-end assembly of AuNRs in a variety of solvents and demonstrate that AuNR chaining can be retained upon casting nanocomposite films. By tuning the aspect ratio, polymer-grafted nanorods have been predicted to reconfigurably self-assemble into superstructures with nanosized patterns<sup>18</sup> offering the possibility of assisting or eschewing traditional lithography and contemporary nanoprinting techniques in the fabrication of precise nanoscale devices.<sup>19</sup> Because this is a general strategy, new, flexible devices can be designed by incorporating rod-like particles of variable compositions with the desired function into processable films, thereby establishing a new class of materials with tunable properties based on metal-nanorod/polymer nanocomposites.

Previous work by our group focused on dispersing AuNRs in polymers by grafting a polymer brush that is either chemically

Received: November 27, 2013

Revised: January 29, 2014

Published: January 31, 2014

similar or exhibits a favorable interaction with the matrix.<sup>15,17,20</sup> The optical properties of the AuNRs are imparted to the polymer film and can be tuned by controlling the local assembly and orientation of the AuNRs. In this work, we present a novel, solution-based method to synthesize bifunctional gold nanorods (B-NRs), assemble them end-to-end in a wide variety of solvents, and disperse the linked B-NRs within a polymer matrix. This strategy takes advantage of the facet dependent surface chemistries of AuNRs that allows for tuning rod–solvent or rod–matrix interactions and opening up new media (i.e., organic) for solubilizing the AuNRs. Furthermore, by exploiting the weak attraction between cysteine and the end of the AuNR, the AuNRs are assembled and dissembled by simply changing solvent and have tunable end grafting that allows for the addition of a functional ligand or polymer between cysteine molecules. By choosing a dithiol ligand, the end-to-end assembly of AuNRs in a wide array of organic solvents and, for the first time, in polymer matrices is demonstrated. Using discrete dipole approximation (DDA) calculations and UV/visible spectroscopy, the optical properties, in solution and polymer matrices, are finely tuned by controlling the linker length, B-NR chain length, and polydispersity. Finally, quartz crystal microbalance with dissipation (QCM-D) is used to determine the role of the cysteine and dithiol in the linking mechanism that chains AuNRs together.

## ■ EXPERIMENTAL SECTION

**Linked B-NR Preparation.** Reagents used in the synthesis were purchased from Sigma-Aldrich and used as received. Polymers were used as received and obtained from Polymer Source, Inc., unless otherwise noted. Three 40 mL solutions of CTAB coated gold nanorods in DI water are synthesized by a seed-mediated growth method as outlined elsewhere.<sup>6,7,17</sup> Excess CTAB is removed through three washing cycles consisting of centrifugation (20 min at 8000 rpm, Eppendorf 5804) followed by replacement of the supernatant with approximately 40 mL of Milli-Q water. Following the washing steps, the three nanorod solutions are combined and concentrated in 40 mL of water, providing a stock solution of concentrated AuNRs.

End linking is performed by centrifuging 5 mL of the stock solution, removing the supernatant, and combining with 9 mL of a 400 mM NaCl solution. Three 3 mL aliquots are taken from the solution, combined with 30  $\mu$ L of a 2 mM L-cysteine solution, and left overnight to end-link.

Upon completion of the previous reaction, the solutions are sonicated for several seconds to redisperse the AuNRs. End-linked AuNRs are then functionalized with 5 kg/mol poly(ethylene glycol) methyl ether thiol (Sigma Aldrich) by adding 30 mg of the polymer to the solutions of end-linked nanorods, centrifuging for 20 min, and replacing the supernatant with 3 mL of methanol or ethanol. Two additional washing steps are performed, and precipitate dispersed in chloroform. Using a similar procedure, we found a PEO grafting density of 0.5 chains/nm<sup>2</sup> on homogeneously grafted AuNRs.<sup>21</sup>

Dithiol and monothiol functionalization was performed by preparing a stock solution of diluted di/monothiol ligand containing 50  $\mu$ L of dithiol to 5 mL of chloroform. 100  $\mu$ L of this stock solution is then added to the solution containing the B-NRs. For kinetics experiments, 1/10th the concentration of linker as above was used. Samples were prepared for SEM by spincasting at 3k RPM onto a silicon wafer, and SEM images were taken on a JEOL 7500F HRSEM. Dithiol functionalization has successfully been performed in a variety of solvents including methanol, ethanol, MEK, and chloroform. In order to use these other solvents, a simple solvent exchange is performed in a similar manner as above. UV/vis spectroscopy was done at each step with a Cary 5000 UV-vis-NIR system.

**Cysteine-Coated Gold Nanosphere Synthesis.** Gold nanospheres of diameter 16  $\pm$  2.8 nm are synthesized following a procedure

as laid out by McFarland et al. with no alterations.<sup>22</sup> Once the spheres are prepared, 5 mL of the solution centrifuged and the supernatant discarded. The concentrated gold particles are then added to 3 mL solution of a 400 mM NaCl solution. Ten microliters of 2 mM cysteine is then added. The solution is left overnight. Finally, solvent exchange is performed by centrifuging the solution and replacing the supernatant with 40 mL of ethanol.

**Thin Film Preparation.** A solution containing the linked B-NRs is first solvent exchanged to chloroform. Once in chloroform, 1.0 wt % of 7.8 kg/mol PEO or 2.1 kg/mol PMMA is then added to this solution and dissolved. Finally, this solution is spin-cast directly onto a Si wafer at 3000 rpm for imaging and drop cast onto a glass slide to measure optical absorption.

**QCM-D Experiments.** The QCM-D measurement is based on the resonance frequency change of a vibrating quartz crystal, a piezoelectric material, when mass is deposited on it. The deposited mass,  $\Delta m$ , has a relationship with the frequency change,  $\Delta f$ , according to the Sauerbrey equation<sup>23–27</sup>

$$\Delta m = -C \frac{\Delta f_n}{n}$$

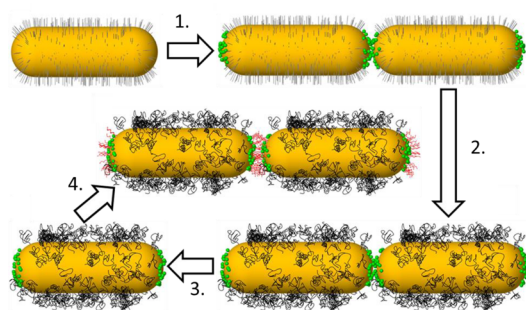
where  $C$  is the mass sensitivity constant ( $C = 17.7 \text{ ng cm}^{-2} \text{ Hz}^{-1}$  for an AT-cut, 5 MHz crystal) and  $n$  is the vibrational mode number ( $n = 1, 3, 5, \dots$ ). In addition, the dissipation change,  $\Delta D_n$ , which is a measure of the loss of energy stored in a vibration cycle, indicates the physical characteristics of the deposited layer such as viscosity, elasticity, and so on. If  $\Delta D_n$  is less than  $2.0 \times 10^{-6}$  and the plots of  $\Delta f_n/n$  under several modes are superimposed, the layer is an elastic film. The physical properties (mass and thickness) of the elastic layer can be calculated using the Sauerbrey equation.<sup>26,27</sup> On the contrary, if  $\Delta D_n$  is more than  $2.0 \times 10^{-6}$  and the plots of  $\Delta f_n/n$  are not superimposed, the layer is viscoelastic. The physical properties (thickness, shear modulus, and viscosity) of the viscoelastic layer can be estimated by fitting between the QCM-D experimental data ( $\Delta f_n/n$  ( $n = 1, 3, 5, \dots$ ) and  $\Delta D_n$ ) and a Voigt-based viscoelastic model incorporated in Q-Sense software Q-Tools.<sup>23,24,27</sup>

Stock solutions of C6DT, cysteine, and cysteine-capped Au nanospheres (C-AuNPs) in ethanol are prepared. Briefly, 10  $\mu$ L of C6DT is added to 40 mL of ethanol, 100  $\mu$ L of 2 mM cysteine is added to another 40 mL of ethanol, and preparation of the C-AuNP stock solution is described above. An E4 QCM instrument (Q-Sense Inc., Gothenburg, Sweden) was used to monitor the binding of cysteine, C6DT, and C-AuNPs to gold-coated QCM sensor crystals. Prepared solutions were pumped by peristaltic pump at a rate of 20  $\mu$ L/min through a flow cell containing the sensor crystal. The temperature of the system was fixed at 21 °C.

**DDA Calculations.** Discrete dipole approximation (DDA) calculations were performed to determine the extinction efficiencies of dimers and tetramers of AuNRs (42 nm  $\times$  12 nm) immersed in a polystyrene matrix as a function of the interparticle separation and wavelength using DDSCAT 7.1 compiled with Open MP support.<sup>28,29</sup> The extinction efficiency ( $Q_{ext}$ ) is the sum of the scattering and absorption efficiencies,  $Q_{scat}$  and  $Q_{abs}$ , respectively. The criterion for accuracy within 5% is that  $|mlkd| < 0.05$ , where  $m$  is the complex refractive index,  $k$  is the wavenumber, and  $d$  is the effective particle size. For our calculations, the gold is embedded in a matrix with average refractive index of 1.55. Dielectric data were obtained from Weaver et al.<sup>30</sup> and corrected for surface damping due to collisions of electrons with the surface of the nanorods.<sup>8,31</sup> The extinction efficiencies were determined by taking the average value for light polarized parallel and perpendicular to the length of the nanorods.

## ■ RESULTS AND DISCUSSION

**Functionalization and Assembly of B-NRs in Solution and Polymer Matrices.** Scheme 1 shows the four steps to prepare and end-to-end-link the bifunctional AuNRs (B-NRs). The CTAB-coated AuNRs are synthesized by methods discussed elsewhere.<sup>6,7,20</sup> First, the ends of the CTAB-coated

Scheme 1<sup>a</sup>

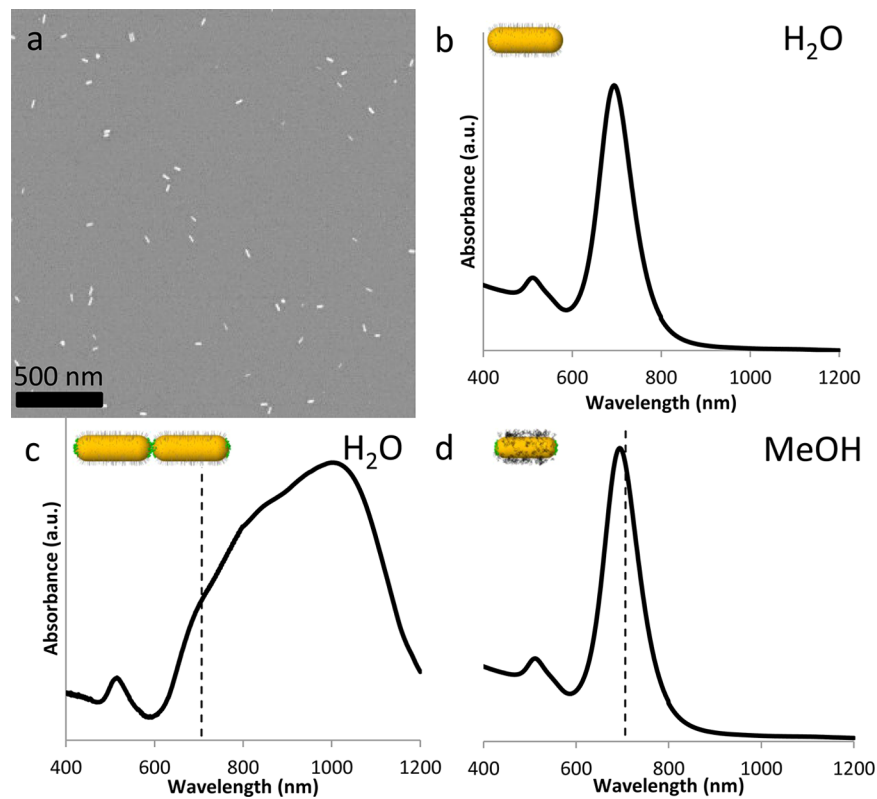
<sup>a</sup>Synthesis proceeds clockwise from the top left. CTAB-coated AuNRs are linked with cysteine (Step 1). CTAB is replaced with HS-PEO (Step 2) to facilitate transfer to non-aqueous solvents. A solvent exchange from water to methanol is performed (Step 3), which delinks the B-NRs and frees up surface binding sites to allow for further end-functionalization. B-NRs are then linked with DT molecules in an organic solvent (e.g., chloroform) (Step 4) and chains of B-NRs can then be transferred to polymer films via simple techniques such as spin-casting.

AuNRs are modified by cysteine, which links the AuNRs in water as shown in step 1. In step 2, the B-NRs are formed by replacing the CTAB along the sides of the AuNRs by a thiol-end functionalized poly(ethylene oxide) brush (HS-PEO). In step 3, the aqueous solution is exchanged with an organic

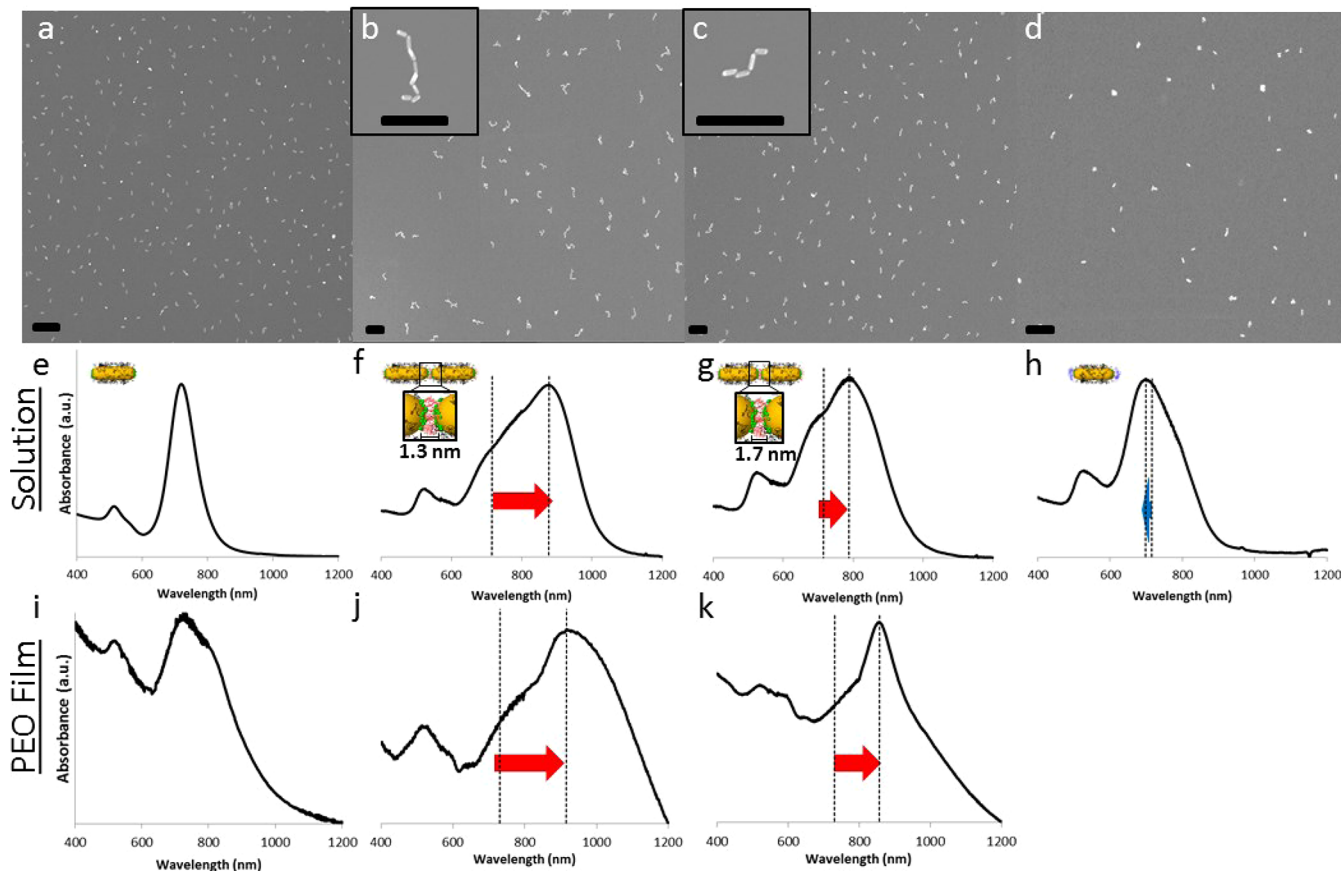
solvent, resulting in the delinking of the B-NRs, and, in step 4, the B-NRs in organic solvent are linked together by end-attached alkane dithiol molecules (DT). Details of each step are described next.

Figure 1a shows a representative SEM image of CTAB-coated AuNRs, which have a length and diameter of  $39.1 \pm 5.1$  nm and  $12.5 \pm 1.4$  nm, respectively, and an aspect ratio (AR) of 3.1. Figure 1b shows the UV/vis spectrum of these AuNRs in water. The longitudinal surface plasmon resonance (LSPR) peak wavelength is 707 nm, consistent with the literature for AuNRs with AR 3.1.<sup>32</sup> The transverse surface plasmon resonance (TSPR), determined by the AuNR diameter, is observed at 536 nm.

The CTAB-coated rods are then linked with cysteine, an amino acid (Scheme 1, step 1), using a modified procedure from the literature.<sup>10</sup> Whereas CTAB inhibits attachment along the side of the AuNR, cysteine binds to the ends of the AuNRs via the thiol moiety. Cysteine is thought to link AuNRs together either by hydrogen bonding<sup>34</sup> or because of its free amino group, the cysteine can link the AuNRs together via an electrostatic interaction.<sup>10</sup> Regardless of linking mechanism, further modification at the ends of the AuNRs is suppressed. Upon linking, Figure 1c shows that the LSPR peak broadens and undergoes a strong red-shift to 1024 nm compared to the CTAB-coated AuNRs (dashed line). This red-shift is due to increased plasmon coupling between the AuNRs, whereas the broadening results from both increased coupling and



**Figure 1.** (a) Representative scanning electron microscope (SEM) image of AuNRs spin-cast from water onto a silicon substrate. The AuNRs are 39 nm long by 12.5 nm in diameter, which results in an aspect ratio of approximately 3.1. This aspect ratio is consistent with the LSPR peak of 707 nm seen in the UV/vis spectra (b). Linking with cysteine results in a strong red-shift and broadening in the LSPR band, shifting the peak to 1024 nm as can be seen in spectra (c), where the dotted line shows the unlinked peak position. The spectra returns to the discrete AuNR case after the CTAB on the side of the AuNR is replaced with 5 kg/mol HS-PEO and the solution is solvent exchanged to methanol with a peak position of 694 nm (d), nearly identical to the discrete AuNRs in water. The small blue shift is most likely due to a change in the index between water and methanol ( $n_{H_2O} > n_{MeOH}$ ).<sup>32,33</sup>



**Figure 2.** Representative SEM images of B-NRs unlinked (a), linked with C6DT (b), linked with C9DT (c), and incubated with 1-octanethiol (d) (all scale bars are 250 nm). B-NRs are well dispersed in the unlinked case (a) and the 1-octanethiol case (d), whereas in the linked cases (b and c) chains of end-linked B-NRs can be clearly seen. UV/vis spectroscopy was performed on solutions of unlinked B-NRs (e), B-NRs linked with C6DT (f) and C9DT (g), and B-NRs incubated with 1-octanethiol (h). A strong red-shift and LSPR peak broadening is seen for linked B-NRs (f and g) as compared to the discrete case (e), while B-NRs incubated with 1-octanethiol exhibit a small blue-shift. UV-visible spectroscopy was also performed on PEO films of B-NRs unlinked (i) and linked with C6DT (j) and C9DT (k). Spectra from the films compare favorably with those taken in solution.

convolution of LSPR peaks from individual, pairs, triads, etc., of AuNRs. This strong red-shift, broadening, and peak location are consistent with literature values for cysteine linked AuNRs.<sup>10</sup>

Because the ends of AuNRs are protected, a thiol-terminated polymer can be introduced to selectively replace CTAB molecules along the side of the AuNR as shown in Scheme 1, step 2. In this study, the CTAB is replaced by a hydrophilic polymer brush, HS-PEO with a molecular weight of 5 kg/mol in aqueous solution. Brush molecular weight is a tunable parameter and assemblies have been demonstrated utilizing a HS-PEO brush with a larger molecular weight of 10 kg/mol. In step 3 of Scheme 1, the solvent is exchanged from water to methanol or ethanol, resulting in the delinking of the AuNRs denoted by the blue shift of the LSPR peak to 694 nm as shown in Figure 1d. The small blue shift, relative to isolated AuNRs in water, occurs due to the lower index of refraction of methanol versus water. Nevertheless, the peak position of dispersed AuNRs in methanol is very similar to that observed for the CTAB-coated AuNRs in water denoted by the dotted line in Figure 1d and the solid line in Figure 1b.

Due to their hydrophilic PEO side and cysteine ends, B-NRs are a versatile building block for hierarchical assembly, in part because the B-NRs disperse in solvents that dissolve PEO. In particular, the B-NRs are adaptable for further end-functionalization. Dithiol (DT) molecules have been used to link

CTAB-coated AuNRs in mixed aqueous/organic solvents.<sup>9</sup> In the present study, 1,6-hexanedithiol (C6DT) and 1,9-nonanedithiol (C9DT) are attached to the ends of the B-NRs (Scheme 1, step 4) to demonstrate control over the end-to-end separation and optical properties of linked B-NRs in solutions and films. Figure 2a–c shows SEM images of unlinked B-NRs and B-NRs incubated with C6DT and C9DT, respectively, for three hours, deposited on silicon. The UV/vis spectra for the dispersed, C6DT linked and C9DT linked B-NRs in solution are given in Figure 2e–g, respectively. For the dispersed B-NRs, the LSPR peak is at 716 nm (c.f. Figure 1b,d). Upon adding C6DT and C9DT, the peak red-shifts to 878 and 789 nm, respectively, and broadens, consistent with end-linking. This UV-vis behavior is supported by the SEM images in Figure 2b,c, which shows chains with an average number of B-NRs of  $5.5 \pm 2.2$  and  $3.0 \pm 1.2$  rods per chain for C6DT and C9DT, respectively. Systematic studies of linker length on chaining of B-NRs are needed to understand difference in chain length between C6DT and C9DT linked B-NRs. To determine if linking is possible without the dithiols, B-NRs are also incubated with an alkane monothiol, 1-octanethiol, for 24 h. Relative to dispersed B-NRs, Figure 2h shows that the LSPR peak undergoes a small blue shift from 716 to 699 nm and slightly broadens. The SEM images in Figure 2d show that the

B-NRs are mainly isolated with a few pairs of side-by-side B-NRs, which accounts for the small blue-shift in Figure 2h.

Polymer nanocomposite films containing end-to-end linked B-NRs in a PEO matrix were prepared by mixing the B-NRs with C6DT or C9DT in an organic solvent containing 1 wt % PEO (7.8 kg/mol), incubating for 3 h to allow linking of B-NRs, and finally drop-casting the solution onto glass slides. For comparison, a solution of unlinked B-NRs in an organic solvent containing 1 wt % PEO was also drop-cast onto a glass slide. Figure 2i–k shows the absorbance spectra for films containing unlinked B-NRs, B-NRs linked by C6DT, and B-NRs linked by C9DT, respectively. For the unlinked B-NR system, the LSPR peak position is 731 nm. This small red-shift relative to the solution case (c.f. Figure 2e, 716 nm) is attributed to the change in refractive index and/or some aggregation of B-NRs upon drying. In contrast, relative to the unlinked B-NR system, the LSPR peak positions undergo a significant red-shift to 916 and 857 nm for the C6DT and C9DT linked B-NR systems, respectively. Table 1 summarizes the absorbance peak positions

**Table 1. LSPR Peak Positions of Unlinked and Linked AuNRs**

surface functionalization	solvent or polymer	LSPR peak (nm)
CTAB	H <sub>2</sub> O	707
Cysteine	H <sub>2</sub> O	1024
HS-PEO	Methanol	694
HS-PEO	CHCl <sub>3</sub>	716
1-octanethiol	CHCl <sub>3</sub>	699
C6DT	CHCl <sub>3</sub>	878
C9DT	CHCl <sub>3</sub>	789
HS-PEO	PEO	731
C6DT	PEO	916
C9DT	PEO	857

at each step during the surface modification and linking process. LSPR peak positions in PEO films are similar to those found in solution suggesting that the linking in solution is retained in the drop-cast film.

**Inter-Rod Spacing, B-NR Chain Length, and Optical Properties.** To interpret the experimental results, the extinction efficiencies ( $Q_{ext}$ ) and LSPR peak position of end-to-end aligned AuNRs were determined from discrete dipole approximation (DDA) calculations. Figure 3a shows  $Q_{ext}$  for pairs of AuNRs (42 nm × 12 nm, AR = 3.5) at separations of 100, 10, and 1 nm, as well as  $Q_{ext}$  for a tetramer having an equal spacing of 1 nm. At a separation of 100 nm (red), plasmonic coupling between AuNRs is weak because the gap is much greater than the nanorod size. Thus, the LSPR peak position is sharp and located at 844 nm, consistent with the aspect ratio of 3.5. As the gap between pairs decreases, Figure 3a shows that the LSPR peak red-shifts to 880 and 959 nm for separations of 10 nm (blue) and 1 nm (black), respectively. The LSPR peaks also broaden as the gap decreases. For the tetramer at 1 nm separation (black dashed), Figure 3a shows that the LSPR peak position undergoes a very strong red-shift to 1064 nm as well as further broadening, compared to discrete AuNRs (red). This strong red-shift and broadening is attributed to increased coupling as the number of “linked” AuNRs increases.

These DDA calculations support the experimental studies of the LSPR peak shifts and broadening reported in Figure 2 and Table 1. The DDA calculations show a stronger shift between discrete rods and the tetramer case, 220 nm, as compared with

discrete B-NRs and those linked with C6DT, 162 nm, despite a similar average chain size (5.5B-NRs per chain). This discrepancy is resolved by realizing that the distance between B-NRs linked with C9DT is almost twice the gap size in the DDA calculation, 1.7 nm compared with 1 nm, resulting in weaker coupling between the B-NRs and a smaller shift.<sup>8</sup> Furthermore, DDA calculations assume that rods are perfectly parallel to each other, whereas in the films, the B-NRs are not perfectly aligned because the linker (i.e., –CH<sub>2</sub>– units) is flexible and rods interacting at angles exhibit weaker longitudinal plasmon coupling.<sup>8,35</sup> This comparison illustrates the sensitivity of optical properties to small changes in linker length and stiffness and suggests a simple route to fine-tune the extinction. For example, by replacing the flexible alkane with a stiff phenyl backbone, end-to-end alignment between B-NRs would increase and correspondingly a larger red-shift would result.

Absorbance spectra in solution predict the assembly of AuNRs after casting into films. B-NRs were linked by incubating in chloroform containing C6DT and poly(methyl methacrylate) (PMMA). PMMA (2.1 kg/mol) was chosen as a matrix to demonstrate that matrix polymers in addition to PEO (Figure 2) are possible. A lower concentration of C6DT, as compared with our previous experiments, was chosen to decrease the reaction kinetics to more precisely analyze the linking behavior of B-NRs. Absorbance spectra from the solution were acquired as a function of incubation time and plotted in Figure S1 (Supporting Information). After incubating the B-NRs with C6DT for a range of times, films were spin-cast from these solutions and then imaged by SEM to correlate the LSPR peak shift and relative broadening with the number and polydispersity of linked B-NRs. Figure 3b shows selected absorbance spectra from the solutions that were used to cast films. Figure 3c shows that the fraction of pairs, triads, etc., of B-NRs increases as incubation time increases, in qualitative agreement with the increasing LSPR peak position red-shift (c.f. Figure 3b) and DDA calculations (c.f. Figure 3a). For example, after 90 min, the percentage of individual B-NRs decreased to 76%, whereas the pairs and triad fraction increased to 14% and 5%, respectively. Figure 3d shows that the number averaged B-NRs per chain ( $X_n$ ) increases linearly plotted against the LSPR peak shift toward the red, consistent with literature.<sup>36</sup> Figure 3e shows that the polydispersity index (PDI) of linked B-NRs increases with time, consistent with a step-growth polymerization mechanism where a wide variety of chain sizes will be present at any given time due to the independence of ‘monomer’ (i.e., B-NRs in this case) reactivity from chain size.<sup>37,38</sup> This increase in PDI correlates with an increase in the fwhm of the LSPR peak that results from the overlap of individual peaks due to pairs, triads, tetramers, etc. In conclusion, these studies show that the LSPR in polymer nanocomposites can be varied by controlling inter-rod spacing between B-NRs (peak position), B-NR  $X_n$  (peak position and breadth), and B-NR PDI (peak breadth). By tailoring nanorod linking, a novel route toward tuning the optical properties of polymer nanocomposite films has been demonstrated here.

**Mechanism for AuNR Assembly.** To understand and better control the assembly of B-NRs, the mechanism for linking B-NRs end-functionalized with dithiol molecules was investigated using QCM-D. In step 1 of Scheme 1, the ends of the AuNRs are modified with cysteine resulting in linking. In this step, the addition of salt screens the self-interaction between the carboxylic and amine groups on the cysteine

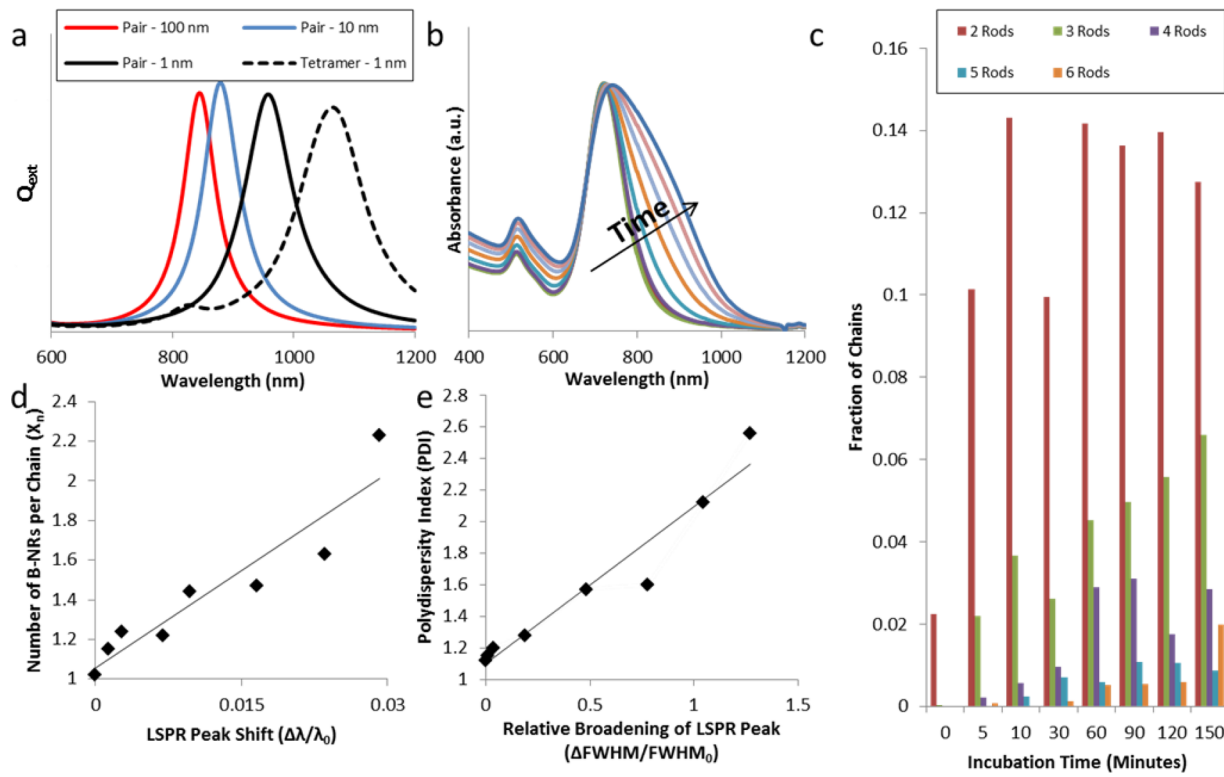


**Figure 3.** (a) DDA calculations for end-linked rods in a polymer matrix. Calculations were performed for pairs of rods at end-to-end separation distances of 100 nm, 10 nm, and 1 nm and for a tetramer of rods at 1 nm. As the distance decreases, the LSPR peak red-shifts and broadens. B-NRs were incubated with C6DT and absorbance spectra were taken at various time points (b). The LSPR peak red-shifts and broadens as a function of time. This solution was cast in a PMMA film at the same time points as the UV/vis data and chain length was analyzed with SEM. (c) As incubation time increases, the average number of B-NRs per chain ( $X_n$ ) also increases.  $X_n$  is correlated with LSPR peak shift (d) which is consistent with DDA calculations. Polydispersity in chain size (PDI) also increases with incubation time and this is correlated with the relative broadening of the LSPR peak (e). The trendlines in d and e serve as guides to the eye.

molecules. Upon solvent exchanging from water to m/ethanol (step 2), the electrostatic interaction weakens and the soluble salt concentration decreases, resulting in a delinking of AuNRs. A corresponding decrease in the grafting density of the cysteine allows for subsequent attachment of DT molecules at the ends of the AuNRs. However, the cysteine grafting density is sufficient to allow only one end of the DT to attach (i.e., no loops form). Because it is longer than the short cysteine, the DT molecule can extend its free SH group to bind with the end of a neighboring AuNR. As incubation time increases, the number of end-to-end linked AuNRs increases as previously observed in Figure 3b.

QCM-D is an in situ method for quantifying the coverage of molecules or particles. The resonance frequency of the quartz crystal substrate decreases as molecules/particles adsorb from the surrounding fluid onto the surface. For elastic layers, this frequency change is related to mass uptake using the Sauerbrey equation. To mimic the functionalization of the end of the AuNR, a gold-coated QCM-D crystal was exposed to the treatments described in Scheme 1. First, the assembly of elastic layers of cysteine and C6DT on the gold-coated crystal was investigated. A monolayer of cysteine was measured and found to have an areal density of 1.94 molecules/nm<sup>2</sup>, consistent with the literature.<sup>39</sup> The areal density of C6DT on the gold crystal was found to be only 0.16 molecules/nm<sup>2</sup>, significantly lower than 4.7 molecules/nm<sup>2</sup> reported for alkane monothiols.<sup>40</sup> This submonolayer coverage indicates that both ends of C6DT can

bind to the gold surface, limiting further attachment of C6DT.<sup>41</sup>

The mechanism of linking was investigated by exposing the planar gold-coated crystal to the scheme in Figure 4a which mimics the steps to link AuNRs depicted in Scheme 1. First, after an exposure time of 40 min and rinsing, cysteine is bound to the gold-coated crystal at a surface coverage of about 50%, similar to the coverage on the ends of AuNRs after delinking. Figure 4b shows the areal mass determined from the QCM frequency (Figure S2, Supporting Information) using the Sauerbrey equation, where the white and gray regions represent the elastic adlayers of cysteine and cysteine/dithiol, and the viscoelastic adlayer of the AuNPs grafted to the cysteine/dithiol layer. After rinsing to remove loosely bound molecules, the areal density of cysteine is 1.12 molecules/nm<sup>2</sup>, about half a monolayer. Upon exposing the submonolayer of cysteine to C6DT, the mass increases rapidly and then more slowly after ~100 min, reaching an areal density of 3.4 C6DT molecules/nm<sup>2</sup> after rinsing. Compared to the areal density of C6DT molecules grafted directly to gold, the cysteine primed surface allows for nearly a 2000% increase, suggesting that cysteine directs C6DT to only end attach rather than form a loop on the gold surface. However, this grafting density is about 30% less than literature values for similarly lengths of alkane monothiols,<sup>25</sup> consistent with cysteine blocking surface sites.

To mimic step 4 in Scheme 1, the planar gold crystal surface is functionalized with a mixture of cysteine and C6DT and then exposed to cysteine-coated spherical AuNPs (16 nm in

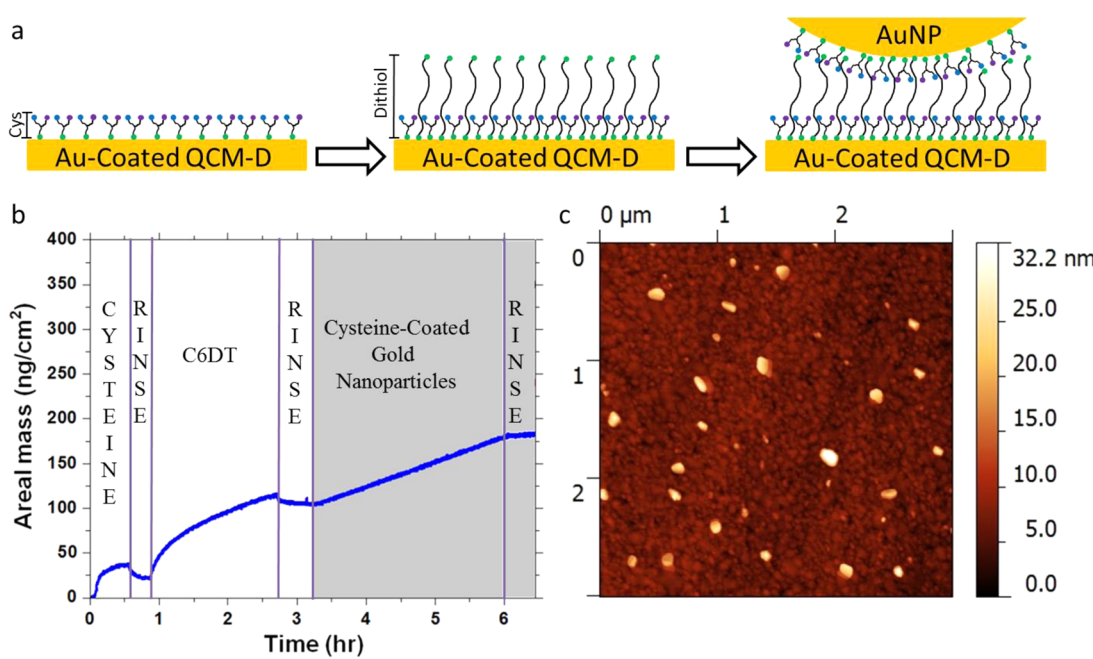


**Figure 4.** (a) Cartoon depicting each step in QCM-D experiments. A gold QCM-D crystal is first coated with a submonolayer of cysteine (cys), followed by C6DT, which binds at interstitial sites between cysteine molecules. Cysteine coated gold nanoparticles (16 nm in diameter) then bind to the gold substrate via C6DT that “stands up”. (b) details the change in areal mass as calculated from the change in frequency of the 7th mode at each step in the QCM-D experiment detailed in (a). Binding events are characterized by an increase in the areal mass. Rinsing steps were done to remove physically bound molecules. Cysteine bound at a density of 1.12 chains/nm<sup>2</sup>, while C6DT bound at 3.4 chain/nm<sup>2</sup>. Cysteine-coated gold nanoparticles were calculated to bind at 18.5 NPs/μm<sup>2</sup>. AFM was performed (c) on the QCM-D crystal and particles with an average feature height of 18.2 ± 5 nm were bound at an areal density of 7 ± 3.

diameter) for approximately three hours as described in Figure 4a. Because they are tethered to the crystal, the AuNP layer is viscoelastic as evidenced by the splitting of the harmonics and increase in dissipation shown in Figure S2 (Supporting Information). For comparison, the cysteine and cysteine/C6DT layers show overlapping harmonics and negligible splitting consistent with an elastic solid. To limit overestimating the NR mass when applying the Sauerbrey equation to viscoelastic films, the harmonic with the lowest dissipation value ( $n = 7$ , c.f. S2, Supporting Information) was used to determine the areal mass and NP areal density at long times, namely, 160 ng/cm<sup>2</sup> and 18.5 NPs/μm<sup>2</sup>, respectively. For a random closed-packed arrangement of noninteracting, spherical, monodisperse AuNPs, the maximum areal density is about 2500 NPs/μm<sup>2</sup>. Thus, the QCM-D measurements indicate a AuNP coverage of about 1% of the ideal maximum packing.

AFM was used to verify the AuNP coverage determined by QCM-D. Figure 4c shows a topography image (3 μm × 3 μm) of the same surface used in the QCM-D experiments described in Figure 4b. The isolated high features (white) are about 1 nm apart and have a height of 18.2 ± 5 nm. This height is consistent with the diameter measured by SEM, 16 nm. For comparison, an AFM image of a neat gold-coated QCM-D crystal was also measured and found to be featureless (Figure S3, Supporting Information). The areal coverage of AuNPs is 7 ± 3 NPs /μm<sup>2</sup>. Given the sparse coverage and resulting error, the direct space AFM results are in agreement with the more sensitive measurement by QCM-D. To summarize, based upon the QCM-D and AFM results, after an initial submonolayer of cysteine forms on the Au surface, C6DT is able to insert itself into the cysteine layer and bind by one end to the gold surface. Moreover, because the cysteine blocks the C6DT from forming

a loop on the surface, a free thiol end extending from the surface can bind with a neighboring AuNP in solution or, in the case of AuNRs, link together nanorods.

**Conclusions.** Herein, we have demonstrated a robust method to synthesize B-NRs, link end-to-end with DT molecules, and disperse, while linked, in a PEO or PMMA matrix. Using a combination of methods including DDA, UV-vis, and SEM, the chain length, inter-rod distance, and chain polydispersity are shown to affect the optical properties of the nanocomposite films. Through UV-vis and QCM-D experiments, the mechanism for B-NRs to be further modified with thiolated molecules has been elucidated. Namely, one end of the DT inserts into the cysteine adlayer on the end of the B-NR and bonds with the end of the B-NR leaving a free thiol to bond with the end of a neighboring B-NR. The links between B-NRs are retained in various solvents and even persist after spin coating solutions to create a polymer nanocomposite film. The UV-vis studies show that the LSPR peak shift is consistent with those predicted by DDA calculations for end-to-end pairs and tetramers of AuNRs at various separation distances. By changing the length of the linker and incubation time, absorption can be tuned both in solution and, for the first time, in a polymer matrix. This latter ability is particularly important because the gap directly determines the strength of plasmonic coupling. By understanding the mechanism that controls linking of B-NRs, side-by-side assembly is also possible by selecting different end and side group molecules, to further tune absorption. Using liquid crystal molecules on the ends, the gap between nanorods can itself become functional and impart additional liquid crystal properties superimposed on those of the metallic nanorods. The anisotropic surface chemistry examined in this study can be expanded to other nanometric

"building blocks" to create unique nanostructures such as controlling the faces of attachment for nanocubes.<sup>42</sup> Thus, the advances in understanding how to direct the assembly of complex particles within a polymer can now be applied to create novel optical, electronic, and sensory devices.

## ■ ASSOCIATED CONTENT

### § Supporting Information

S1: UV/vis spectra for B-NRs linked with 1,6 hexanedithiol in chloroform at different incubation times. S2: Traces of (top)  $\Delta f_n/n$  ( $n = 3, 5, 7$ ) and (bottom).  $\Delta D_n$  versus time for formation of cysteine submonolayer, followed by formation of 1,6-hexanedithiol/cysteine layer and subsequent nanoparticle grafting. S3: Topography AFM image of neat QCM-D crystal showing no features. S4: Transmission electron micrographs of AuNRs end-linked with cysteine. Samples were drop-cast from water. S5: Absorbance spectra of AuNRs before (blue curve) and after (red curve) replacement of CTAB surfactant layer with 5K HSPEO. A 5 nm red shift can be seen after CTAB is replaced with a homogeneous PEO layer. This material is available free of charge via the Internet at <http://pubs.acs.org>.

## ■ AUTHOR INFORMATION

### Corresponding Author

\*E-mail: composto@seas.upenn.edu.

### Notes

The authors declare no competing financial interest.

## ■ ACKNOWLEDGMENTS

This work was supported by the National Science Foundation with primary support from the Polymer (DMR09-07493) and CEMRI (DMR11-20901) programs. The National Institutes of Health provided support via grant R01 EB006818 (DME). Secondary support was provided by NSF/NSEC (DMR08-32802). The authors acknowledge Dr. J. Ford (University of Pennsylvania) for his help with SEM imaging.

## ■ REFERENCES

- (1) Qian, X.; Li, J.; Nie, S. Stimuli-Responsive SERS Nanoparticles: Conformational Control of Plasmonic Coupling and Surface Raman Enhancement. *J. Am. Chem. Soc.* **2009**, *131*, 7540–7541.
- (2) Nihoobakht, B.; El-Sayed, M. Surface-Enhanced Raman Scattering Studies on Aggregated Gold Nanorods. *J. Phys. Chem. A* **2003**, *107*, 3372–3378.
- (3) Zhang, X.; Liu, H.; Tian, J.; Song, Y.; Wang, L. Band-Selective Optical Polarizer Based on Gold-Nanowire Plasmonic Diffraction Gratings. *Nano Lett.* **2008**, *8*, 2653–2658.
- (4) Canfield, B. K.; Kujala, S.; Jefimovs, K.; Vallius, T.; Turnen, J.; Kauranen, M. Polarization Effects in the Linear and Nonlinear Optical Responses of Gold Nanoparticle Arrays. *J. Opt. A* **2005**, *7*, 110–117.
- (5) Merlein, J.; Kahl, M.; Zuschlag, A.; Sell, A.; Halm, A.; Boneberg, J.; Leiderer, P.; Leitenstorfer, A.; Bratschitsch, R. Nanochemical Control of an Optical Antenna. *Nat. Photonics* **2008**, *2*, 230–233.
- (6) Nikoobakht, B.; El-Sayed, M. A. Preparation and Growth Mechanism of Gold Nanorods (NRs) Using Seed-Mediated Growth Method. *Chem. Mater.* **2003**, *15*, 1957.
- (7) Sau, T. K.; Murphy, C. J. Seeded High Yield Synthesis of Short Au Nanorods in Aqueous Solution. *Langmuir* **2004**, *20*, 6414.
- (8) Funston, A. M.; Novo, C.; Davis, T. J.; Mulvaney, P. Plasmon Coupling of Gold Nanorods at Short Distances and in Different Geometries. *Nano Lett.* **2009**, *9*, 165.
- (9) Joseph, S. T. S.; Ipe, B. I.; Pramod, P.; Thomas, K. G. Gold Nanorods to Nanochains: Mechanistic Investigations on Their Longitudinal Assembly Using  $\alpha,\omega$ -Alkanedithiols and Interplasmon Coupling. *J. Phys. Chem. B* **2006**, *110*, 150–157.
- (10) Sethi, M.; Joung, G.; Knecht, M. R. Linear Assembly of Au Nanorods Using Biomimetic Ligands. *Langmuir* **2009**, *25*, 1572–1581.
- (11) Caswell, K. K.; Wilson, J. N.; Bunz, U. H. F.; Murphy, C. Preferential End-to-End assembly of Gold Nanorods by Biotin-Streptavidin Connectors. *J. Am. Chem. Soc.* **2003**, *125*, 13914–13915.
- (12) Chang, J.; Wu, H.; Chen, H.; Ling, Y.; Tan, W. Oriented Assembly of Au Nanorods Using Biorecognition System. *Chem. Commun.* **2005**, 1092–1094.
- (13) Sudeep, P. K.; Joseph, S. T. Shibu; Thomas, K. G. Selective Detection of Cysteine and Glutathione Using Gold Nanorods. *J. Am. Chem. Soc.* **2005**, *127*, 6516–6517.
- (14) Nie, Z.; Fava, D.; Kumacheva, E.; Zou, S.; Walker, G. C.; Rubinstein, M. Self-Assembly of Metal-Polymer Analogues of Amphiphilic Triblock Copolymers. *Nat. Mater.* **2007**, *6*, 609–614.
- (15) Hore, M. J. A.; Fischknecht, A. L.; Composto, R. J. Nanorod Assemblies in Polymer Films and Their Dispersion-Dependent Optical Properties. *ACS Macro Lett.* **2012**, *1*, 115–121.
- (16) Sun, Z.; Ni, W.; Yang, Z.; Kou, X.; Li, L.; Wang, J. pH-Controlled Reversible Assembly and Disassembly of Gold Nanorods. *Small* **2008**, *9*, 1287–1292.
- (17) Hore, M. J. A.; Composto, R. J. Using Miscible Polymer Blends to Control Depletion-Attraction Forces Between Au Nanorods in Nanocomposite Films. *Macromolecules* **2012**, *45*, 6078–6086.
- (18) Nguyen, T. D.; Glotzer, S. C. Reconfigurable Assemblies of Shape-Changing Nanorods. *ACS Nano* **2010**, *4*, 2585–2594.
- (19) Chanda, D.; Shigeta, K.; Gupta, S.; Cain, T.; Carlson, A.; Mihi, A.; Baca, A. J.; Bogart, G. R.; Braun, P.; Rogers, J. A. Large-area Flexible 3D Optical Negative Index Metamaterial Formed by Nanotransfer Printing. *Nat. Nanotechnol.* **2011**, *6*, 402–407.
- (20) Hore, M. J. A.; Composto, R. J. Nanorod Self-Assembly for Tuning Optical Absorption. *ACS Nano* **2010**, *4*, 6941–6949.
- (21) Fischknecht, A. L.; Hore, M. J. A.; Ford, J.; Composto, R. J. Dispersion of Polymer Grafted Nanorods in Homopolymer Films: Theory and Experiment. *Macromolecules* **2013**, *46*, 2856–2869.
- (22) McFarland, A. D.; Haynes, C. L.; Mirkin, C. A.; Van Duyne, R. P.; Godwin, H. A. Color My Nanoworld. *J. Chem. Educ.* **2004**, *81*, 544A.
- (23) Lee, H.; Penn, L. S. In Situ Study of Polymer Brushes as Selective Barriers to Diffusion. *Macromolecules* **2008**, *41*, 8124–8129.
- (24) Jhon, Y. K.; Bhat, R. R.; Jeong, C.; Rojas, O. J.; Szleifer, I.; Genzer; Salt-Induced Depression of Lower Critical Solution Temperature in a Surface-Grafted Neutral Thermoresponsive Polymer. *J. Macromol. Rapid Commun.* **2006**, *27*, 697–701.
- (25) Sauerbrey, G. Z. Phys. **1959**, *155*, 206–222.
- (26) Vogt, B. D.; Lin, E. K.; Wu, W.; White, C. C. Effect of Film Thickness on the Validity of the Sauerbrey Equation for Hydrated Polyelectrolyte Films. *J. Phys. Chem. B* **2004**, *108*, 12685–12690.
- (27) Hook, F.; Kasemo, B.; Nylander, T.; Fant, C.; Sott, K.; Elwing, H. Variations in Coupled Water, Viscoelastic Properties, and Film Thickness of a Mefp-1 Protein Film During Adsorption and Cross-Linking: A Quartz Crystal Microbalance with Dissipation Monitoring, Ellipsometry, and Surface Plasmon Resonance Study. *Anal. Chem.* **2001**, *73*, 5796–5804.
- (28) Flatau, P. J. Discrete Dipole Approximation for Scattering Calculation. *J. Opt. Soc. Am. A* **1994**, *11*, 1491.
- (29) Draine, B. T.; Flatau, P. J. User Guide to the Discrete Dipole Approximation Code DDSCAT 7.1 2010; arXiv.org e-print archive; <http://arXiv.org/abs/1002.1505v1> (accessed 2012).
- (30) Weaver, J.; Kafka, C.; Lynch, D.; Koch, E. Physics Data: Optical Properties of Metals, Part 2: Noble Metals, Aluminum, Scandium, Yttrium, the Lanthanides and the Actinides; Fach-Informations Zentrum: Karlsruhe, 1981.
- (31) Ungureanu, C.; Rayavarapu, R. G.; Manohar, S.; van Leeuwen, T. G. Discrete Dipole Approximation Simulations of Gold Nanorod Optical Properties: Choice of Input Parameters and Comparison with Experiment. *J. Appl. Phys.* **2009**, *105*, 102032.
- (32) Link, S.; Mohamed, M. B.; El-Sayed, M. A. Simulation of the Optical Absorption Spectra of Gold Nanorods as a Function of Their

Aspect Ratio and the Effect of the Medium Dielectric Constant. *J. Phys. Chem. B.* **1999**, *103*, 3073–3077.

(33) Chen, H.; Kou, X.; Yang, Z.; Ni, W.; Wang, J. Shape- and Size-Dependent Refractive Index Sensitivity of Gold Nanoparticles. *Langmuir* **2008**, *24*, 5233–5237.

(34) Ni, W.; Mosquera, R. A.; Perez-Juste, J.; Liz-Marzan, L. M. Evidence for Hydrogen-Bonding-Directed Assembly of Gold Nanorods in Aqueous Solution. *J. Phys. Chem. Lett.* **2010**, *1*, 1181–1185.

(35) Shao, L.; Woo, K. C.; Chen, H.; Jin, Z.; Wang, J.; Lin, H.-Q. Angle and Energy-Resolved Plasmonic Coupling in Gold Nanorod Dimers. *ACS Nano* **2010**, *4*, 3053–3062.

(36) Liu, K.; Ahmed, A.; Chung, S.; Sugikawa, K.; Wu, G.; Nie, Z.; Gordon, R.; Kumacheva, E. In Situ Plasmonic Counter for Polymerization of Chains of Gold Nanorods in Solution. *ACS Nano* **2013**, *7*, 5901–5910.

(37) Odian, G. *Principles of Polymerization*, 4th ed., 2004; p 41.

(38) Liu, K.; Nie, Z. H.; Zhao, N. N.; Li, W.; Rubinstein, M.; Kumacheva, E. Step-Growth Polymerization of Inorganic Nanoparticles. *Science* **2010**, *329*, 197–200.

(39) Zhang, J.; Chi, Q.; Nielsen, J. U.; Friis, E. P.; Andersen, J. E. T.; Ulstrup, J. Two-Dimensional Cysteine and Cystine Cluster Networks on Au(111) Disclosed by Voltammetry and in Situ Scanning Tunneling Microscopy. *Langmuir* **2000**, *16*, 7229–7237.

(40) Strong, L.; Whitesides, G. M. Structures of Self-Assembled Monolayer Films of Organosulfur Compounds Adsorbed on Gold Single Crystals: Electron Diffraction Studies. *Langmuir* **1988**, *4*, 546–558.

(41) Leung, T. Y. B.; Gertsenberg, M. C.; Lavrich, D. J.; Scoles, G.; Schreiber, F.; Poirier, G. E. 1,6-Hexanedithiol Monolayers on Au(111): A Multitechnique Structural Study. *Langmuir* **2000**, *16*, 549–561.

(42) Gao, B.; Arya, G.; Tao, A. R. Self-orienting Nanocubes for the Assembly of Plasmonic Nanojunctions. *Nat. Nanotechnol.* **2012**, *7*, 433–437.